Aging Determination of Lithium Ion Batteries Based on Thermal Measurements

Joanna Kozma, Khadija El Kadri Benkara, Rabih Dib, Christophe Forgez, Nazih Moubayed, Guy Friedrich

Aging Determination of Lithium Ion Batteries Based on Thermal Measurements

Joanna Kozma
Roberval (Mechanics, Energy and Electricity)
University of Technology of Compiegne
Compiegne, France
joanna.kozma@utc.fr

Khadija El Kadri Benkara
Roberval (Mechanics, Energy and Electricity)
University of Technology of Compiegne
Compiegne, France
khadija.el-kadri-benkara@utc.fr

Rabih Dib
LaRGES, Faculty of Engineering
Lebanese University
Tripoli, Lebanon
Rabih.Dib@ul.edu.lb

Christophe Forgez
Roberval (Mechanics, Energy and Electricity)
University of Technology of Compiegne
Compiegne, France
christophe.forgez@utc.fr

Nazih Moubayed
LaRGES, Faculty of Engineering
Lebanese University
Tripoli, Lebanon
nazih.moubayed@ul.edu.lb

Guy Friedrich
Roberval (Mechanics, Energy and Electricity)
University of Technology of Compiegne
Compiegne, France
guy.friedrich@utc.fr

***Abstract*— Lithium-ion batteries (LIBs) are the most widely used electrical energy storage devices in various application areas. Since aging reduces their performance, it is important to diagnose this phenomenon. Currently, the aging of LIBs is determined either by destructive methods or by methods that depend on electrical components. In our study, we were able to diagnose the state of aging of the battery using calorimetry, which requires thermal measurements. The temperature profile can be used as an indicator of the aging state. This can be considered as a simple and effective way without the need for costly and/or destructive analysis.**

Keywords*— *Lithium-ion Batteries (LIBs), aging, calorimetry, thermal measurement.

I. INTRODUCTION

Batteries are devices that convert chemical energy into electrical energy through electrochemical reactions and are used to store electrical energy. Their importance is increasing more and more nowadays as they are used in several application areas such as electronic products, automotive, aerospace and military industries. In particular, LIBs are considered to be the battery technology of choice due to their high energy density, high voltage, low self-discharge rate, wide operating temperature range, and lack of memory effect [1], [2]. However, one of the main drawbacks of LIBs is their aging, which is due to several internal and external factors [3]. Battery aging generally manifests itself in the form of a decrease in capacity and an increase in the internal impedance. This aging effect limits their performance, reduces their autonomy and lifespan and can even lead to certain safety risks [4]. It is therefore essential to perform an aging diagnosis to avoid problems related to this phenomenon.

Several diagnosis methods have been studied in the literature. The post-mortem analysis method, reported by [5]–[7], consists of disassembling aged batteries and observing each battery component to determine the aging mechanisms by analyzing the materials inside. However, this work requires great care to avoid internal short circuit and other safety related issues as well as contamination. This makes this method complicated and involves irreversible destruction of the batteries. The method based on electrochemical impedance spectroscopy (EIS), used by [8]–[10], studies the aging of batteries in a non-destructive way. The EIS consists in applying a sinusoidal signal for different frequencies, and measuring a sinusoidal output signal for the same frequencies. Thus, the corresponding internal impedance is calculated from the output amplitude and phase shift. A Nyquist plot showing the impedance value for different frequencies of the battery usually represents the EIS. It is modeled using an equivalent electrical circuit (ECM) where each component of the model corresponds to the different electrochemical phenomena occuring within the battery. Therefore, it is possible to observe a change in the internal resistance of the battery during aging and to analyze the corresponding aging reactions by identifying the ECM parameters.

Incremental capacity analysis (ICA) and differential voltage analysis (DVA) [11]–[14] are diagnostic methods that are inversely related. They allow representing the voltage curve V of the cells as a function of the capacitance Q to highlight the voltage plateaus. These representations are $\mathrm{dQ/dV} = f(V)$ and $\mathrm{dV/dQ} = f(Q)$ for the ICA and DVA curves respectively. For the ICA curve, the peaks indicate the voltage plateaus i.e. the areas where two phases are in equilibrium. While for the DVA curve, the peaks are relative to the state of the electrode where only one phase is encountered. The shape of the curve changes according to the age of the battery enabling the diagnosis of aging.

The previously mentioned works such as EIS, ICA and DVA depend largely on electrical quantities such as resistance, current and voltage of the batteries, while other sources of information are neglected. For this reason, [15]–[17] diagnosed aging from battery surface temperature measurements and voltage measurements. The method they used is differential thermal voltammetry (DTV). It consists in studying the quantity $\mathrm{dT/dV} = f(V)$. DTV curves form peaks related to phase transitions of the electrode materials, which allows diagnosing aging. However, the data are vulnerable to perturbations in the voltage measurement when the differential voltage (dV) appears in the denominator.

We have seen that there are different techniques for battery aging diagnosis in the literature. However, none of them alone can provide all the information needed to monitor and analyze the degradation mechanisms that occur in a battery. For this reason, researchers combine different techniques to overcome some of the limitations related to each of them. Hence, in this paper, a method is proposed that is able to detect a change in the electrical resistance of the battery due to aging based on calorimetric measurements. This method can serve as an additional tool to supplement other techniques. The method is described in section II. The thermal model is presented in section III. Section IV describes the experimental setup used. The results obtained are shown in section V. The conclusions are presented in section VI.

This work is funded by Hauts-de-France Region and IRP ADONIS.

II. Proposed Method

LIBs can be modeled by an equivalent electrical circuit model (Fig. 1.a) where each component of the model corresponds to different electrochemical phenomena [18] : a voltage source U_{OC} defined as the battery voltage in open circuit (OCV), a series resistance R_s representing the pure resistive contributions (electrolyte, current collectors, contact resistances), a surface resistance R_{surf} corresponding to the potential drop between the surface of active materials and the electrolyte (due to the charge transfer R_{ct} and to the SEI "Solid Electrolyte Interphase"), a capacity C_{surf} representing the capacitif effect of charge transfer and SEI, a diffusion impedance Z_w that encompasses impedances due to charge diffusion in the electrolyte and lithium atoms diffusion in the active material of both electrodes. Those phenomena described earlier are represented by battery impedance characteristic curve (Nyquist diagram) where each point is an impedance measurement at a different frequency (Fig. 1.b).

When battery undergoes aging, this implies an increase in its electrical resistance, which results in an increase in the heating rate.Thus, the relationship between the heating rate and the internal electrical resistance contributing to the heat generation should be exploited.

Initially, we apply the EIS for a new cell to assess its condition. The area of interest of the curve for the aging study corresponds to the semicircle modeling the surface phenomena ($R_{ct} + R_{SEI}$). This area is limited by two characteristic points : point A corresponding to the pure series resistance R_s of the battery and point B corresponding to the sum of R_s with the charge transfer resistance R_{ct} and the SEI resistance R_{SEI}. The heating of the battery is a contribution of the real part of the impedance of both points A and B. First, we apply two charge-discharge current profiles of precise

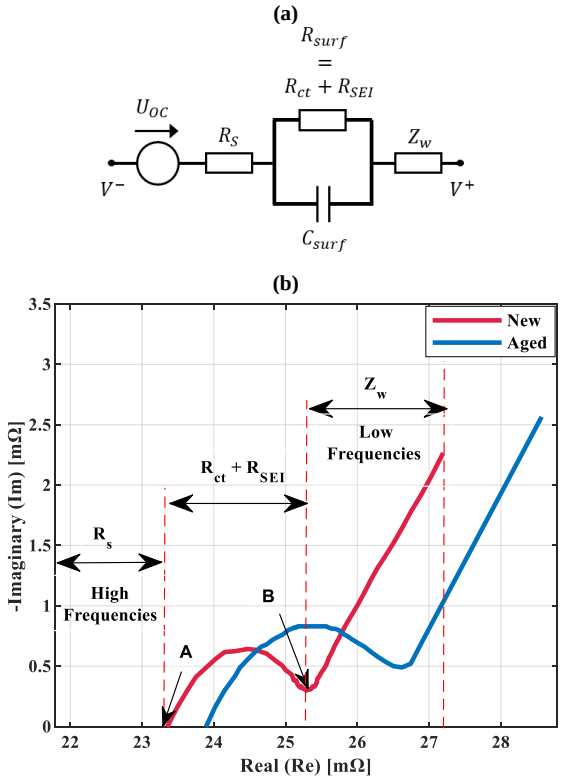

Fig. 1. (a) Electrical circuit model. (b) Nyquist diagram for a new (measured) and aged cell (expected behavior based on literature [3]) for a constant state of charge and ambient temperature.

RMS value for the frequencies of the points A and B. We observe the difference in temperature behavior between these two points of the battery. This first step informs us about the possibility of detecting a variation in the temperature profile between these two points. The temperature response for a new battery at points A and B will be a "signature" of the condition of the battery before its aging. Second, after the cell has undergone aging, we observe the temperature profiles of the battery for the same frequencies as points A and B and with the same applied RMS current (noting that frequencies may change slightly between new and aged batteries). The resulting change in temperature profile will be a simple indicator of the aging process.

III. Thermal Model

A. Thermal model presentation

We begin by presenting the simplified equivalent circuit (Fig. 2.a) of the cell and its corresponding lumped thermal model. This model is used by [19]:

$$\dot{Q} = C_{th}\frac{dT_{in}}{dt} + \frac{T_{in} - T_s}{R_{in}} = C_{th}\frac{dT_{in}}{dt} + \frac{T_s - T_{amb}}{R_{out}} \quad (1)$$

where C_{th} is the thermal capacity that represents the accumulation of thermal energy within the battery, R_{in} identifies the heat exchange between the core of the battery and its surface, R_{out} identifies the heat exchange between the surface of the battery and its environment, T_{in} is the internal temperature of the battery, T_s is the surface temperature of the battery, T_{amb} is the temperature of the ambient air and $\dot{Q}$ is the heat generated by the battery. Equation (1) includes several unkown variables ($\dot{Q}, C_{th}, T_{in}, R_{in}, R_{out}$) to be determined which requires additional experimental measurements. Since the aim of this work is to determine the aging of the cell from a simple measurement of the surface temperature, simplifications to this circuit must be made.

To do that , we isolated our cell thermally. Thus, by wrapping the cell with insulating material, the first simplification is to consider R_{in} negligible compared to R_{out} which allows to have $T_{in} \simeq T_s$ (homogeneous battery temperature). The thermal model becomes a single node model (Fig. 2.b) composed of two parameters (R_{th} and C_{Th}) and governed by (2) :

$$\dot{Q} = C_{th}\frac{dT_s}{dt} + \frac{T_s - T_{amb}}{R_{th}} \quad (2)$$

where R_{th} identifies the heat exchange between the surface of the battery and its environment. These two parameters will be identified in our work based on the approach used by [20]. We are only interested in the term $C_{Th}(dT_s/dt)$ of the model which corresponds to the heating rate of the battery. The second term of (2) should be neglected. To do so, the first assumption taken into consideration is that the thermal resistance must tend to infinity (requirements met using a semi-adiabatic calorimeter). Second assumption is to have a slight temperature difference between the surface of the battery and the environment (requirements met at the beginning of the temperature response curve of the cell).

Furthermore, $\dot{Q}$ is the result of several processes that contribute to heat generation within the battery. Two main heat sources are commonly considered in literature and presented by (3) [21]:

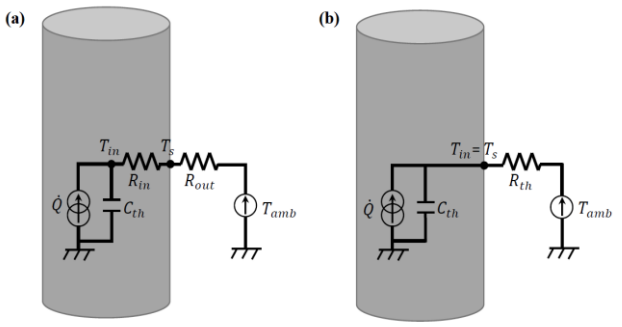

Fig. 2. (a) Simplified thermal model. (b) Thermal model of the cell in semi-adiabatic conditions.

$$\dot{Q} = I(U_{cell} - U_{OC}) + IT\frac{\partial U_{OC}}{\partial T} \quad (3)$$

The first term corresponds to the heat generated by Joule effect, also known as irreversible heat, because it is always positive. U_{cell} is the global voltage of the cell and I is the applied current (positive during the charge and negative during the discharge). The second term corresponds to the heat generated by entropy variation, also known as reversible heat, because its sign depends on whether the reaction is endothermic or exothermic. We are only interested in the term $I(U_{cell} - U_{OC})$ corresponding to the heat generated by Joule effect of the model. To eliminate the second term of (3), a judicious choice of current profile (symmetrical charge and discharge) must be applied. Thus, with all these assumptions, the relationship between the temperature slope measurement dT_s/dt and the electrical resistance contributing to the heat generation $\dot{Q}$ is exploited.

B. Heat capacity determination

The heat capacity C_{th} is measured using the setup shown on Fig. 4 (section IV). The cell is covered with polyurethane foam to ensure that the internal thermal resistance (from the cell core to its surface) is negligible compared to the external thermal resistance (from the cell surface to the ambient air). This is important to respect the assumptions of a semi-adiabatic condition. A ± 10 A (± 2 C) current with a period T of 10 s has been applied to the cell around the same state of charge (SoC) to create a heat generation step. The duration of the period is very small compared to the thermal time constant of the cell and it allows a sufficient heat generation rate. This allows us to have an average current that is equal to zero and thus have an average reversible heat that is also equal to zero. Therefore, only electrical losses contribute to the heating of the cell. In this way, we can consider that U_{OC} is constant. In addition, at the very beginning of the test, the difference between T_s and T_{amb} is very small due to semi-adiabatic conditions. Therefore, the last term in (2) can be neglected. The heat capacity can be determined by (4):

$$C_{th} \simeq \frac{\int_{t_1}^{t_2} I(U_{cell} - U_{oc})dt}{T_s(t_2) - T_s(t_1)} \quad (4)$$

Where the current I and the cell voltage U_{cell} are measured during the test, U_{OC} is measured before beginning the test, when the cell was at an equilibrium state. C_{th} has been found to be equal to 61 $J.K^{-1}$ approximately. The specific heat capacity C_p is calculated by dividing the heat capacity with the mass of the cell. Its value is found to be equal to 884 $J.K^{-1}.kg^{-1}$.Based on literature, specific heat values vary according to the battery technology used. We found a range value of 840 to 1180 $J.K^{-1}.kg^{-1}$ for NMC technology [22],[23].

C. Thermal resistance determination

We adopted the same experimental setup used for the determination of the heat capacity. We fully charged the battery by the constant current constant voltage (CCCV) method and left it to rest until reaching its thermal equilibrium. We applied the following protocol: fully discharge the cell by a constant current and leave it to rest, then fully charge it and leave it to rest. The temperature evolution and the applied current of value ± C/3 are shown in Fig. 3.a and Fig. 3.b respectiveley. The thermal resistance R_{th} has been determined during the first rest period (3h to 6.5h). In these conditions, the total heat generation is assumed to be equal to zero. Consequently, (2) can be simplified to (5).

$$C_{Th}\frac{dT_s}{dt} + \frac{T_s - T_{amb}}{R_{th}} = 0 \quad (5)$$

We used fmincon, an optimization tool on MATLAB, to minimize the error between experimental data and fitted data to obtain the best fit . The optimal value for R_{th} has been found to be equal to 68.3 $K.W^{-1}$.

IV. Experimental Setup

The cell chosen in our work is the LG INR21700 M50 using $LiNi_8Co_1Mn_1O_2$ (NMC811) as cathode material and graphite-silicon blend (C + SiO_y) as anode material, with a nominal capacity of 5 Ah and a mass of 69 g. To insure semi-adiabatic conditions, the cell was placed in the center of a polyurethane insulator as shown in Fig. 4.a. We placed a T-type thermocouple and a PT100 temperature sensor to measure the surface temperature of the battery. Thermal paste was used to minimize the contact resistance between the battery surface and the temperature sensors. Kapton thermal tape was used to attach the sensor to the cell's surface (Fig. 4.b). The thermal resistance of the calorimeter was estimated analytically and determined experimentally to validate the thermal assumptions considered. The semi-adiabatic calorimeter is placed in a thermal chamber to regulate and control the external temperature (Fig. 4.c).

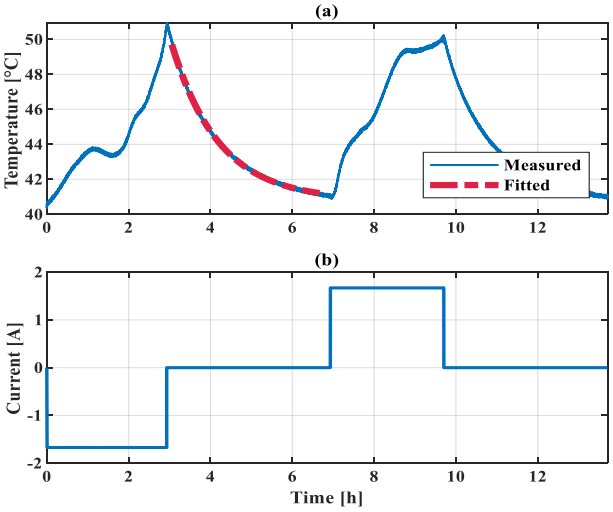

Fig. 3. (a) Cell temperature response due to the applied current. (b) Current profile of C/3 (1.67 A) applied during the discharge-rest-charge-rest protocol.

A BioLogic system was used as the measuring device and source of current or voltage. This is composed of a VSP-120 which drives the VMP3B-20 current amplifier used in our work. This 20 A amplifier delivers a voltage of ±20 V. The BioLogic system is also capable of performing impedance measurements. To monitor and have another source of data, a YOKOGAWA data acquisition system (DL850E) was used to record the voltage and current data. A Graphtec GL220 data logger was also used to record the temperature data measured with the thermocouple. A Tektronix A6302 current measurement probe with an accuracy of 3% is connected to a current amplifier. The latter is connected to the data acquisition system used to record the voltage and current data. This was with the aim of having another source of data and to be able to monitor accurately.

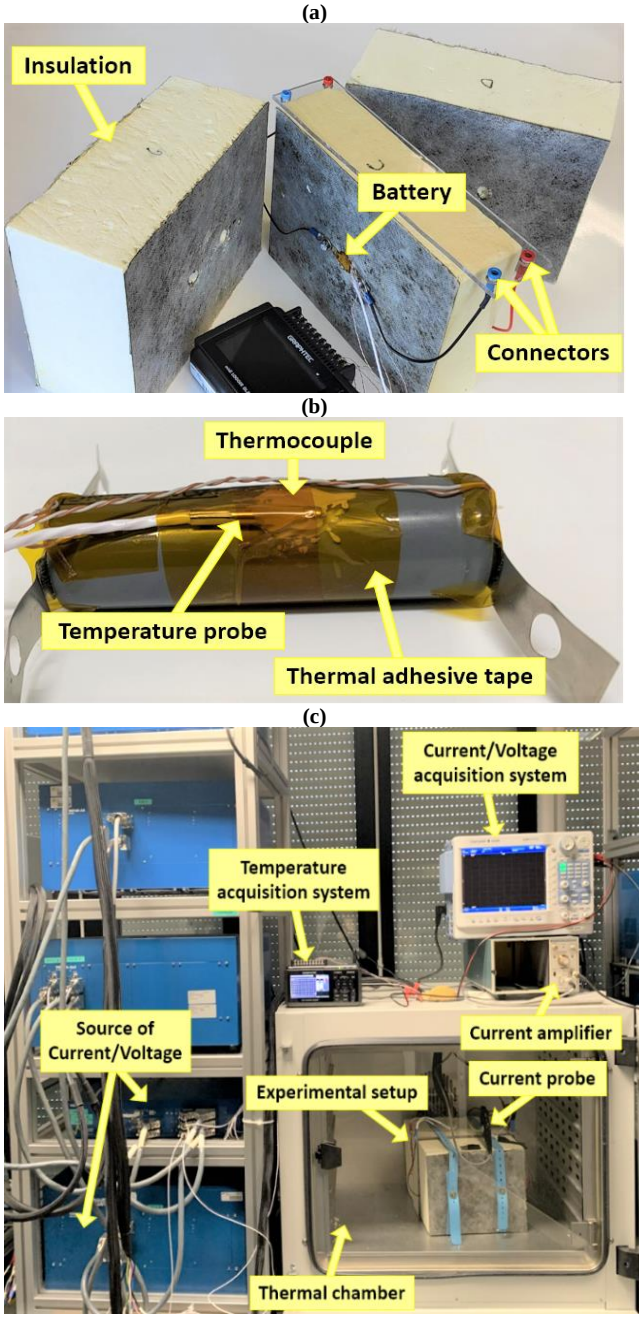

Fig. 4. (a) Location of the battery inside the semi-adiabatic calorimeter. (b) Position of the temperature sensors on the battery. (c) Experimental setup.

V. Results

All tests and results presented in the following section were carried out for :

- an initial battery temperature of 25°C (climatic chamber control temperature of 25°C);
- a constant SoC of 50% ;
- a battery for a new and aged state of health (SoH).

To achieve battery aging, 58 cycles were applied. These cycles were performed at a constant reference temperature of 0°C. This choice of temperature was taken to speed up aging, as shown in [22]. Each cycle includes a discharge, a rest phase and a charge. The value of the current applied during charging and discharging is ±1 C. The charge and discharge cycles were limited by two conditions : the cut-off voltages from 4.2 V to 2.7 V and the durations used for the charge and discharge phases, which were 15 min and 20 min respectively. The battery reached an SoH of 92% (aged state). Low temperature has caused the battery to age in comparison with a rather low number of cycles applied. According to the supplier's data sheet, the battery achieves the same SoH for 400 cycles, at 24°C, for a current of ±0.33 C and cut-off voltages of 4.2 V/ 2.85 V during charging and discharging respectively.

The first step was to apply the EIS technique. The obtained results are presented on Fig. 5. The red and blue curves represent the EIS results for the cell at 100% and 92% SoH, respectively. The series and surface resistances for the battery are represented by points A and B. The indexes N and A refer to the condition of the battery: new and aged. We could observe a change in both resistances for the two different battery states, which is normal since this is the usual trend in battery evolution. The frequency and resistance values corresponding to points A and B for the two battery states are shown in TABLE I.

The second step was to subject the battery to a sinusoidal current of RMS value C/2 (2.5 A) at the frequencies already obtained. The battery begins to heat up. The increase in temperature over time is shown in Fig. 6. The solid and dashed red curves show the temperature evolution corresponding to the series resistances (A_N) and surface resistances (B_N) respectively for the battery in new condition. While the solid and dashed blue curves show the temperature evolution corresponding to the series resistances (A_V) and surface resistances (B_V) respectively for the battery in aged condition.

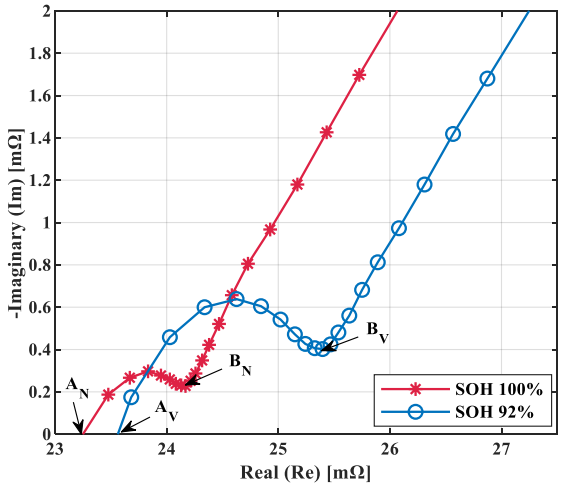

Fig. 5. Nyquist diagram for the battery in new and aged conditions.

The part of the curve we are interested in is the linear part at the beginning of the heating process (shown by the zoomed part of Fig. 6) to approach adiabatic conditions. The calculation time range is from 2 min to 4 min. The obtained results were averaged over this time interval. The obtained slope results are equal to 9.91 °C/h for point B_V, 9.74 °C/h for point B_N, 9.06 °C/h for point A_V and 8.91 °C/h for point A_N. The results obtained for slope values are in the same range as those obtained by impedancemetry. These results are modest, both in terms of resistance and heating rate.

TABLE I. FREQUENCIES AND IMPEDANCES OBTAINED AT POINTS A AND B FOR A NEW AND AGED STATE OF THE BATTERY (SOC=50% et T_{amb}=25 °C).

Variables	SoH 100%		SoH 92%	
	A_N	B_N	A_V	B_V
Re (mΩ)	23.24	24.17	23.51	25.40
Im (mΩ)	0	0.23	0	0.40
f (Hz)	193.09	8.21	228.03	5.53

In order to verify the accuracy of the diagnosis method we used in the current work, it is necessary to calculate and compare the heat generation at points A and B using two different methods. The first method determines the heat generation from calorimetric measurements based on the thermal model of the cell (heat capacity being already calculated). The second method determines heat generation through the product of the internal resistance and the square of the RMS current ($R_s I_{eff}^2$ et $(R_s + R_{ct} + R_{SEI})\, I_{eff}^2$ for points A and B respectively) based on impedancemetry.

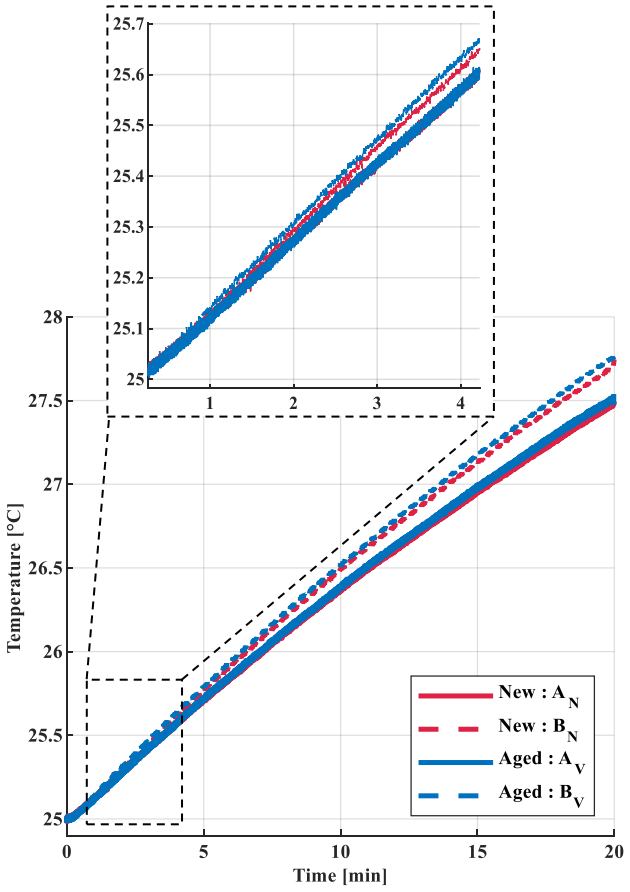

Fig. 6. Temperature response obtained at points A and B for a new and aged state of the battery (SOC=50% et T_{amb}=25 °C).

TABLE II shows the results obtained for both methods. The obtained values show a good agreement between the two measurement methods. We obtained a difference ranging from 3% to 8%, which is less than 10%. This represents a satisfactory result.

TABLE II. HEAT GENERATION FOR BOTH POINTS A AND B FOR THE BATTERY IN NEW AND AGED CONDITIONS (SOC=50% et T_{amb}=25 °C).

Measurement methods	Heat generation (mW) SOH = 100%		Heat generation (mW) SOH = 92%	
	A_N	B_N	A_V	B_V
Electrical	145	151	147	159
Calorimetry	151	165	153	168
Difference between the two methods	3.80%	8.45%	4.26%	5.44%

VI. CONCLUSIONS

The aim of this study was to propose a method capable of detecting a change in the internal electrical resistance of the battery due to aging based on calorimetric measurements. This method can be considered a simple laboratory-based tool for aging diagnosis, since it is based on surface temperature measurement using thermocouples, without the need for costly or destructive analysis. It focuses on the first part of the temperature curve evolution, which corresponds to the first few minutes of the experiment, without having to wait for hours to reach a steady state of the cell. We were able to observe an increase in the rate of battery heating, corresponding to an increase in the series and surface resistances of the cell. A comparison between heat generated by calorimetric and electrical methods was also carried out, to determine the accuracy with which we obtained our aging diagnosis results. The difference obtained was less than 10%, showing good agreement between the two methods. The work is still in progress, and several aging protocols must be taken into consideration to obtain more significant results. A number of parameters also need to be taken into account, such as the applied current rate, the state of charge and the external temperature, to be able to carry out an on-line diagnosis of the cell. It is also necessary to see whether this method can be applicable in on-board applications and not just under calorimetric conditions.

ACKNOWLEDGMENT

We thank the Hauts-de-France Region and the IRP ADONIS for their funding of this research work. The IRP ADONIS is an international research project between four French and Lebanese partners: the University of Technology of Compiegne, the Lebanese University (Faculty of Engineering), the CNRS France and the CNRS Lebanon.

REFERENCES

[1] T. M. Bandhauer, S. Garimella, and T. F. Fuller, "A Critical Review of Thermal Issues in Lithium-Ion Batteries," *J Electrochem Soc*, vol. 158, no. 3, p. R1, 2011, doi: 10.1149/1.3515880.

[2] M. Armand *et al.*, "Lithium-ion batteries – Current state of the art and anticipated developments," *J Power Sources*, vol. 479, Dec. 2020, doi: 10.1016/j.jpowsour.2020.228708.

[3] B. Pan *et al.*, " Aging mechanism diagnosis of lithium ion battery by open circuit voltage analysis," *Electrochim Acta*, vol. 362, Dec. 2020, doi: 10.1016/j.electacta.2020.137101.

[4] R. Xiong, Y. Pan, W. Shen, H. Li, and F. Sun, " Lithium-ion battery aging mechanisms and diagnosis method for automotive applications:

Recent advances and perspectives," *Renewable and Sustainable Energy Reviews*, vol. 131. Elsevier Ltd, Oct. 01, 2020. doi: 10.1016/j.rser.2020.110048.

[5] T. Waldmann *et al.*, "Review—Post-Mortem Analysis of Aged Lithium-Ion Batteries: Disassembly Methodology and Physico-Chemical Analysis Techniques," *J Electrochem Soc*, vol. 163, no. 10, pp. A2149–A2164, 2016, doi: 10.1149/2.1211609jes.

[6] B. Stiaszny, J. C. Ziegler, E. E. Krauß, M. Zhang, J. P. Schmidt, and E. Ivers-Tiffée, " Electrochemical characterization and post-mortem analysis of aged LiMn 2O4-NMC/graphite lithium ion batteries part II: Calendar aging," *J Power Sources*, vol. 258, pp. 61–75, Jul. 2014, doi: 10.1016/j.jpowsour.2014.02.019.

[7] T. Waldmann, M. Wilka, M. Kasper, M. Fleischhammer, and M. Wohlfahrt-Mehrens, "Temperature dependent ageing mechanisms in Lithium-ion batteries - A Post-Mortem study," *J Power Sources*, vol. 262, pp. 129–135, Sep. 2014, doi: 10.1016/j.jpowsour.2014.03.112.

[8] C. Pastor-Fernandez, W. Dhammika Widanage, J. Marco, M. A. Gama-Valdez, and G. H. Chouchelamane, "Identification and quantification of ageing mechanisms in Lithium-ion batteries using the EIS technique," in *2016 IEEE Transportation Electrification Conference and Expo, ITEC 2016*, Jul. 2016. doi: 10.1109/ITEC.2016.7520198.

[9] D. I. Stroe, M. Swierczynski, A. I. Stan, V. Knap, R. Teodorescu, and S. J. Andreasen, "Diagnosis of lithium-ion batteries state-of-health based on electrochemical impedance spectroscopy technique," in *2014 IEEE Energy Conversion Congress and Exposition, ECCE 2014*, Nov. 2014, pp. 4576–4582. doi: 10.1109/ECCE.2014.6954027.

[10] J. Jiang, Z. Lin, Q. Ju, Z. Ma, C. Zheng, and Z. Wang, "Electrochemical Impedance Spectra for Lithium-ion Battery Ageing Considering the Rate of Discharge Ability," in *Energy Procedia*, Elsevier Ltd, 2017, pp. 844–849. doi: 10.1016/j.egypro.2017.03.399.

[11] A. Barai *et al.*, "A comparison of methodologies for the non-invasive characterisation of commercial Li-ion cells," *Progress in Energy and Combustion Science*, vol. 72. Elsevier Ltd, pp. 1–31, May 01, 2019. doi: 10.1016/j.pecs.2019.01.001.

[12] L. Zheng, J. Zhu, D. D. C. Lu, G. Wang, and T. He, "Incremental capacity analysis and differential voltage analysis based state of charge and capacity estimation for lithium-ion batteries," *Energy*, vol. 150, pp. 759–769, May 2018, doi: 10.1016/j.energy.2018.03.023.

[13] D. I. Stroe and E. Schaltz, "Lithium-Ion Battery State-of-Health Estimation Using the Incremental Capacity Analysis Technique," in *IEEE Transactions on Industry Applications*, Institute of Electrical and Electronics Engineers Inc., Jan. 2020, pp. 678–685. doi: 10.1109/TIA.2019.2955396.

[14] J. P. Fath *et al.*, "Quantification of aging mechanisms and inhomogeneity in cycled lithium-ion cells by differential voltage analysis," *J Energy Storage*, vol. 25, Oct. 2019, doi: 10.1016/j.est.2019.100813.

[15] B. Wu, V. Yufit, Y. Merla, R. F. Martinez-Botas, N. P. Brandon, and G. J. Offer, "Differential thermal voltammetry for tracking of degradation in lithium-ion batteries," *J Power Sources*, vol. 273, pp. 495–501, Jan. 2015, doi: 10.1016/j.jpowsour.2014.09.127.

[16] Y. Merla, B. Wu, V. Yufit, N. P. Brandon, R. F. Martinez-Botas, and G. J. Offer, "Novel application of differential thermal voltammetry as an in-depth state-of-health diagnosis method for lithium-ion batteries," *J Power Sources*, vol. 307, pp. 308–319, Mar. 2016, doi: 10.1016/j.jpowsour.2015.12.122.

[17] Z. Wang, C. Yuan, and X. Li, "Lithium Battery State-of-Health Estimation via Differential Thermal Voltammetry with Gaussian Process Regression," *IEEE Transactions on Transportation Electrification*, vol. 7, no. 1, pp. 16–25, Mar. 2021, doi: 10.1109/TTE.2020.3028784.

[18] N. Damay, K. Mergo Mbeya, G. Friedrich, and C. Forgez, "Separation of the charge transfers and solid electrolyte interphase contributions to a battery voltage by modeling their non-linearities regarding current and temperature," *J Power Sources*, vol. 516, Dec. 2021, doi: 10.1016/j.jpowsour.2021.230617.

[19] C. Forgez, D. Vinh Do, G. Friedrich, M. Morcrette, and C. Delacourt, "Thermal modeling of a cylindrical LiFePO4/graphite lithium-ion battery," *J Power Sources*, vol. 195, no. 9, pp. 2961–2968, 2010, doi: 10.1016/j.jpowsour.2009.10.105.

[20] N. Damay, C. Forgez, M.-P. Bichat, and G. Friedrich, "A method for the fast estimation of a battery entropy-variation high-resolution curve-Application on a commercial LiFePO4/graphite cell A method for the fast estimation of a battery entropy-variation high-resolution curve-Application on a commercial LiFeP," Elsevier, 2016. [Online]. Available: https://hal.archives-ouvertes.fr/hal-02007386

[21] Z. Y. Jiang, H. B. Li, Z. G. Qu, and J. F. Zhang, "Recent progress in lithium-ion battery thermal management for a wide range of temperature and abuse conditions," *International Journal of Hydrogen Energy*, vol. 47, no. 15. Elsevier Ltd, pp. 9428–9459, Feb. 19, 2022. doi: 10.1016/j.ijhydene.2022.01.008.

[22] P. Jindal, R. Katiyar, and J. Bhattacharya, "Evaluation of accuracy for Bernardi equation in estimating heat generation rate for continuous and pulse-discharge protocols in LFP and NMC based Li-ion batteries," *Appl Therm Eng*, vol. 201, Jan. 2022, doi: 10.1016/j.applthermaleng.2021.117794.

[23] T. S. Bryden *et al.*, "Methodology to determine the heat capacity of lithium-ion cells," *J Power Sources*, vol. 395, pp. 369–378, Aug. 2018, doi: 10.1016/j.jpowsour.2018.05.084.